INSTITUTE OF PHYSICS PUBLISHING JOURNAL OF PHYSICS B: ATOMIC, MOLECULAR AND OPTICAL PHYSICS

J. Phys. B: At. Mol. Opt. Phys. **35** (2002) 543–555 PII: S0953-4075(02)29626-1

Electron impact dissociative excitation of water within the adiabatic nuclei approximation

J D Gorfinkiel, L A Morgan and Jonathan Tennyson

Department of Physics and Astronomy, University College London, Gower Street, London WC1E 6BT, UK

Received 8 October 2001, in final form 30 November 2001
Published 24 January 2002
Online at stacks.iop.org/JPhysB/35/543

Abstract

The *R*-matrix method is used to calculate dissociative excitation cross sections for the four lowest-lying electronically excited states of H_2O in the energy range 5–15 eV. For the first time calculations are performed taking into account the nuclear motion by means of an adaptation of the adiabatic nuclei approximation. Cross sections are compared with previous and new fixed-nuclei results and also experiments. Resonance positions and widths are calculated for different geometries of the water molecule.

1. Introduction

Water is an extremely important molecule: it is the main constituent of living organisms, it is present in the atmosphere, space environments and is a solvent in many chemical processes. The damage caused by ionizing radiation on biological matter, in particular on DNA, has been an important field of experimental research in the last few years (see Boudaiffa *et al* (2000) and references therein). Structural water molecules are always present in living matter and the (secondary) electrons responsible for radiation damage have energies between 1 and 20 eV.

Experimental work on electron–water collisions has been mainly restricted to dissociative attachment (for example, Belič *et al* (1981), Melton (1972), Curtis and Walker (1992)), photodissociation (e.g. Mordaunt *et al* (1994), Hwang *et al* (1999)) and energy-loss spectra (Lassetre *et al* 1968, Trajmar *et al* 1973). Photodissociation has also been extensively studied theoretically (e.g. Engel *et al* (1992), Schinke (1993), Yang *et al* (2000), van Harrevelt and van Hemert (2000b)). Fragmentation of water in the gas phase has been studied experimentally in various ways (e.g. Tsurubichi *et al* (1974), Kurawaki *et al* (1983)) but only recently have measurements of the dissociation of water specifically via electron impact excitation been made available (Harb *et al* 2001). Fragmentation of water in the solid amorphous state has also been studied (Rountree *et al* 1991, Kimmel and Orlando 1995). Few theoretical calculations on dissociative excitation of water are available (Morgan 1998, Gil *et al* 1994, Lee *et al* 1993, Pritchard *et al* 1990) and all these studies neglect nuclear motion.

0953-4075/02/030543+13$30.00

In this paper, we calculate total (integral) cross sections for excitation into the four lowest states of water. We use the R-matrix method and the R-matrix polyatomic code (Morgan *et al* 1997) to deal with the electronic part of the process. To take into account the nuclear motion, we assume that dissociation will proceed into the formation of H and OH and use the energy balancing method (Stibbe and Tennyson 1998a, Trevisan and Tennyson 2001). This method is an adaptation of the adiabatic nuclei (AN) approximation that allows for the features of the dissociation process to be taken into account.

The ionization potential of water is 12.62 eV (NIST 2001): for energies of the incoming electron higher than this value, this process will start to have some importance and so will excitation to other electronic states of water. For this reason, we limit our calculation to 15 eV. For the purpose of comparison, we also calculate cross sections using the fixed-nuclei approximation. Resonance positions and widths are determined for a set of molecular geometries.

All magnitudes are given in atomic units, unless stated otherwise.

2. Method

The basic idea of the R-matrix method is the division of configuration space into two regions. The boundary between the regions is defined by a sphere of a given radius a centred at the centre of mass of the molecule. In the inner region, exchange and correlation are taken into account using rigorous quantum chemistry methods. In the outer region, where these effects are negligible, the use of a long-range multipole potential suffices to describe the electron–molecule interaction. The application of the R-matrix method to polyatomic molecules within the fixed-nuclei approximation has been described in detail elsewhere (Morgan *et al* 1997, 1998).

Previous calculations on electron–water scattering were carried out using the fixed-nuclei approach. This means that nuclear motion was neglected and calculations performed at the equilibrium geometry of the molecule. In order to include the nuclear motion we use the energy balancing method (see Stibbe and Tennyson (1998a), Trevisan and Tennyson (2001)). This method is an extension of the AN approximation (Chase 1956, Hara 1969, Shugard and Hazi 1975) that takes into account that the excess energy of the incoming electron can be split in any proportion between the dissociating fragments and the outgoing electron. It also allows for the inclusion of tunnelling effects.

In this paper, we treat the nuclear dynamics of water as a pseudo-diatomic molecule. In its equilibrium geometry, the length of both O–H bonds is $r_{\mathrm{OH}} = 1.81$ and the angle between them is $\alpha = 104.5^{\circ}$. The ground state equilibrium bond length of OH is 1.83 (NIST 2001). Since these two values are very similar, it is possible to assume that dissociation into H and OH will take place via stretching of a single OH bond. Consequently, in our calculations, we fix one of the O–H bonds and the angle at its equilibrium value and change the other bond length in the range [1.3; 2.6].

In the energy balancing method, off-shell fixed-nuclei T-matrices are calculated for a range of OH distances and then averaged using the initial (bound), $\Xi_{i\nu}(r_{\mathrm{OH}})$, and final (continuum), $\Xi_{jc}(E_{ke}, r_{\mathrm{OH}})$, nuclear wavefunctions:

$$T_{i\nu\rightarrow jc}(E_{\mathrm{in}}, E_{\mathrm{out}}) = \langle \Xi_{jc}(E_{ke}, r_{\mathrm{OH}}) | T_{ij}(\epsilon_j(r_{\mathrm{OH}}) + E_{\mathrm{out}}, E_{\mathrm{out}}, r_{\mathrm{OH}}) | \Xi_{i\nu}(r_{\mathrm{OH}}) \rangle \tag{1}$$

where i and j denote the initial and final electronic states, E_{in} is the energy of the incoming electron, ν denotes the initial vibrational state, E_{ke} and E_{out} are, respectively, the relative kinetic energy of the dissociating fragments and the energy of the scattered electron and $\epsilon_j(r_{\mathrm{OH}})$ corresponds to the energy threshold for excitation into the state j for each value of

r_{OH}. The T_{ij} are purely electronic and are calculated using the standard R-matrix procedure. The total cross section for excitation into each electronic dissociative state is calculated by integrating the energy-differential cross sections over all possible energies of the outgoing electron (in atomic units):

$$\frac{d\sigma_{iv\to jc}}{dE_{out}} = \frac{\mu}{4\pi^3}\frac{E_{ke}}{E_{in}}\sum_{S\Gamma l_i l_j}(2S+1)|T^{S\Gamma}_{ivl_i jcl_j}(E_{in}, E_{out})|^2 \tag{2}$$

where μ is the reduced mass of the system, S is its total spin, Γ defines its spatial symmetry and l_i and l_j are the partial waves associated with the incoming and outgoing channels, respectively. The explicit relation between the $T^{S\Gamma}_{ivl_i jcl_j}$ and $T_{iv\to jc}$ can be found in Trevisan and Tennyson (2001).

The electronic wavefunctions of the system are calculated using standard quantum chemistry methods (see section 3.1). The nuclear ground and continuum vibrational wavefunctions are calculated using the program LEVEL (Le Roy 1996) and directly solving the Schrödinger equation, respectively. The potentials required (that of the ground electronic state of water and those of the different electronic excited states) are explicitly calculated in the range $r_{OH} \in [1.0; 2.6]$ and then extrapolated to 8.0. The ones corresponding to singlet states are extrapolated using the data of van Harrevelt and van Hemert (2000a) and the triplet state potentials using analytical exponential functions. As a test we extended the extrapolation range to 18.0: no significant change in the shape of the wavefunctions was observed.

3. Characteristics of the calculation

3.1. Target states

In order to obtain the target electronic wavefunctions, we first perform a Hartree–Fock self-consistent-field (HF-SCF) calculation using the double-zeta plus polarization (DZP) Gaussian basis set of Dunning (1970) for O and the triple-zeta (TZ) basis of Dunning (1971) for H augmented with a diffuse s function and two p functions extracted from the basis set used by Gil *et al* (1994).

Using the molecular orbitals thus obtained, pseudo-natural orbitals (NOs) for all the target states included in the calculation are generated from configuration interaction (CI) calculations of the order of 35 000 and 55 000 configurations for the singlets and triplets, respectively. To obtain a set of NOs that is good for the representation of all the target states in the whole r_{OH} range, we perform a weighted averaging of them. After several tests, we found that the best choice (i.e. the one that provides the best set of threshold energies and dipole moments for the ground state) is one that includes NOs from the ground state $^1A_1(\tilde{X})$, the $1\ ^3B_1$ and the $^1B_1(\tilde{A})$ with weights 4, 3 and 2, respectively. The same weights are used for all molecular geometries where these states are labelled as $^1A'(\tilde{X})$, $1\ ^3A''$ and $^1A''(\tilde{A})$, respectively[1]. Finally, a CASCI (complete active space configuration interaction: all the possible configurations arising from distributing the electrons among the orbitals in the active space are built) calculation is performed. In our model, the $1a_1$ orbital was doubly occupied and all the excitations in the active space $(2a_1, 3a_1, 4a_1, 5a_1, 1b_1, 2b_1, 1b_2)^8$ were taken into account. Some tests were performed in the direction of using more elaborate models for the target wavefunctions, in particular CASSD. In this model, configurations with single and double excitations from the active space into a limited space of target virtual orbitals are also included. We found that it was impossible to maintain the balance between the N-electron

[1] The water molecule in its equilibrium geometry belongs to the C_{2v} point group. The single-stretch geometries belong to the C_s. Throughout the text, we will make reference to the irreducible representations from both point groups to label the states and orbitals. See table 1 for the correspondence between the two sets of labels.

Table 1. Vertical excitation energy (in eV) for the H_2O target states. Also given are the number of configurations, N, in the CI and excitation values from: (A) van Harrevelt and van Hemert (2000a) and (B) best values from Winter *et al* (1975).

State			Vertical excitation (eV)		
C_{2v}	C_s	N	This paper	A	B
$^1A_1(\tilde{X})$	$^1A'(\tilde{X})$	260	—	—	—
$1\,^3B_1$	$1\,^3A''$	298	7.034	—	7.14
$^1B_1(\tilde{A})$	$^1A''(\tilde{A})$	230	7.508	7.63	7.49
$1\,^3A_1$	$1\,^3A'$	290	9.202	—	9.35
$^1A_1(\tilde{B})$	$^1A'(\tilde{B})$	260	9.855	9.95	9.73
$1\,^3A_2$	$2\,^3A''$	298	12.338	—	
$1\,^3B_2$	$2\,^3A'$	290	12.973	—	9.93
$^1A_2$	$^1A''$	230	13.123	9.60	
$^1B_2(\tilde{E}')$	$^1A'(\tilde{E}')$	260	14.023	11.11	10.0

target representation and the $(N + 1)$-electron collision complex (for a discussion on this problem see Tennyson (1996)) and therefore opted for the CAS model.

The ground state energy for the equilibrium geometry is $-76.092\,30$, which can be compared with the value of van Harrevelt and van Hemert (2000a), -76.2905; the resulting dipole and quadrupole moments are $\mu = 0.7334$ (the experimental value is $\mu = 0.7295$), $Q_0 = 0.026\,56$ and $Q_2 = -1.9715$. Energy differences between the ground and excited states, listed in table 1, are in good agreement with previous calculations.

The same model is used to calculate the target properties for the non-equilibrium geometries (the active space is now $(2a', 3a', 4a', 5a', 6a', 1a'', 2a'')^8$). Fewer results are available for comparison. In the case of the singlet states, van Harrevelt and van Hemert (2000a) performed MRDCI calculations for several states and several geometries. Our threshold energies are compared with their results in figure 1. As can be seen, the agreement is good for the ground state and the two lowest singlet states. In the case of the $^1A''$ and $^1A'(\tilde{E}')$ states our energies are too high over the whole range. These two states are known to be diffuse; in particular, the $2\,^1A''$ state is dominantly of Rydberg character. Since our basis set (and therefore our natural orbitals) has to be contained inside the R-matrix sphere, diffuse states cannot be accurately represented. Nevertheless, we include these states in our calculation (as well as their corresponding triplets) as a way of accounting for the polarization of the target in the presence of the incoming electron.

To our knowledge, and somewhat surprisingly, there appear to be no previous data for the triplet state energies for non-equilibrium geometries.

3.2. Scattering model

We perform the scattering calculations using two models as a way of testing the convergence of our results. Model (*a*) includes seven target states: $^1A'(\tilde{X})$ (ground state), $1\,^3A''$, $^1A''(\tilde{A})$, $1\,^3A'$, $^1A'(\tilde{B})$, $2\,^3A'$, $^1A'(\tilde{E}')$. Model (*b*) includes nine target states: the ones from the previous model plus the $2\,^3A''$ and $^1A''$. For model (*a*) an R-matrix radius of $a = 10$ is sufficient, but inclusion of the diffuse A'' states means that, in order to make sure that all target wavefunctions are contained inside the inner region, $a = 13$ is used for model (*b*).

The continuum orbitals describing the scattered electron are represented using Gaussian type orbitals (GTOs) with $l \leqslant 4$ centred at the molecule centre of mass. The sets of optimized GTOs are obtained by fitting numerical Bessel functions over a finite range (Nestmann and Peyerimhoff 1990) that is usually slightly bigger than that of the R-matrix radius for which

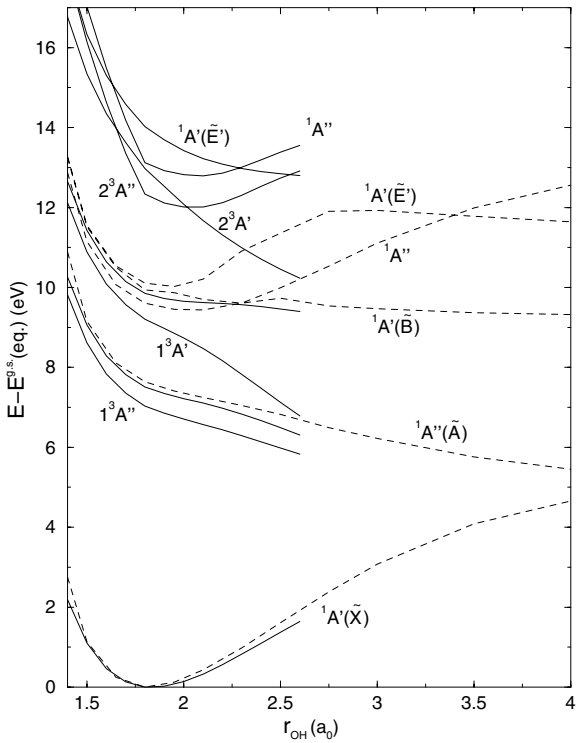

Figure 1. Energies of the nine lowest electronic states of the H_2O as a function of the bond length r_{OH}. The other bond length and the angle between both are kept at their equilibrium values. Full curves, this work; broken curves, data for singlet states (from van Harrevelt and van Hemert 2000a). Energies are defined by setting the ground state equilibrium value of both calculations to zero.

it is going to be used. Since two different radii are used in this work, two sets of continuum GTOs are necessary and we use those presented in Faure *et al* (2001). These GTOs are then orthogonalized to the ones being used for describing the target and only those with an overlap smaller than a certain threshold (in our case 2×10^{-7}) are retained.

4. Results

Since all the previous calculations concerning electron impact dissociative excitation of water used the fixed-nuclei approximation, we will first analyse our fixed-nuclei cross sections as well as the resonances for the equilibrium geometry.

The 1 $^3A''$, $^1A''(\tilde{A})$ and 1 $^3A'$ states dissociate into OH(X $^2\Pi$) + H(1s), that is both fragments in their ground state. Conversely, the state $^1A'(\tilde{B})$ dissociates into the lowest excited state of the hydroxyl, OH(A $^2\Sigma^+$), and the ground state of H. In this last case, the equilibrium bond length of OH, 1.91, differs more significantly from that of water, making our approximation of fixing this distance at 1.81 less satisfactory. Nevertheless, we think that the AN cross section will give some idea of the effect of the nuclear motion on this process. We have tested the inclusion of the Born correction (Chu and Dalgarno 1974): this correction is non-zero only for dipole-allowed transitions and therefore will only affect the cross sections for excitation into the $^1A'(\tilde{B})$ and $^1A''(\tilde{A})$ states. Its maximum effect occurs for the latter at 15 eV where the change in the cross section is smaller than 10%. Consequently, we do not include this correction in the results shown in this section.

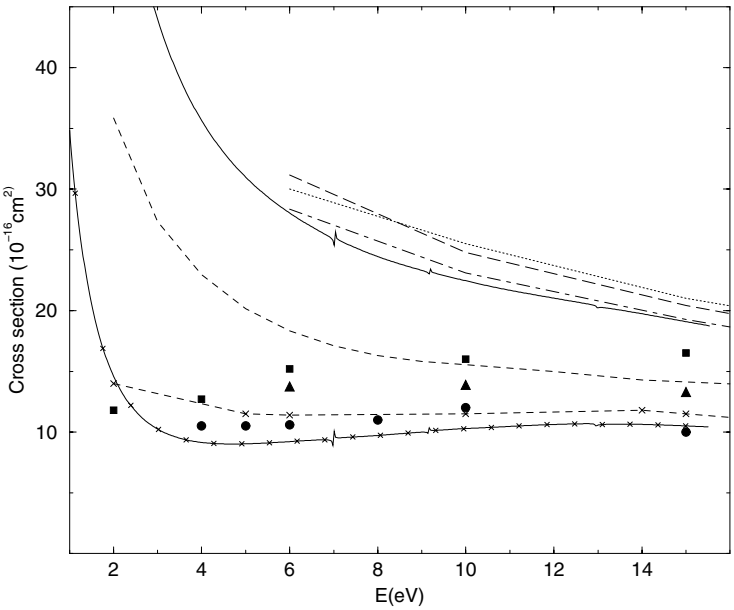

Figure 2. Electronically elastic cross section. Full curve: Born corrected cross section for $J = 0$; full curve with ×: R-matrix elastic cross section with $l \leqslant 4$ and model (*a*); dotted curve: Gianturco *et al* (1998); long-dashed curve: Okamoto *et al* (1993); chain curve: Okamoto *et al* (1993) averaged over rotational-state population; broken curve: Varella *et al* (1999) with Born closure; broken curve with ×: same work without Born closure. Experimental results: triangles: Danjo and Nishimura (1985); circles: Shyn and Cho (1987); full squares: Johnstone and Newell (1991).

Resonance positions and widths are determined using two methods: by fitting the eigenphase sum to a Breit–Wigner profile (Tennyson and Noble 1984) and by fitting the largest eigenvalue of the time-delay matrix using the program TIMEDEL (Stibbe and Tennyson 1998b).

4.1. Fixed-nuclei cross sections and resonances

We investigate the existence of a bound H_2O^- state. No bound states are found for H_2O^- either using the CASCI model or using CASSD or CASSDT (CAS plus single, double and triple excitations) models. Morgan (1998) found a weakly bound state of symmetry $^2A_1$ that is likely to become unbound if rotational motion is taken into account. We therefore conclude that there are no bound states for this system.

Since water is a polar molecule, the elastic cross section is formally divergent in the fixed-nuclei approximation. But it is possible to overcome this using a closure formula that involves the Born approximation (see, for example, Gianturco *et al* (1998)) to calculate cross sections that depend on the initial rotational state.

The resulting cross section for $J = 0$ is plotted in figure 2. Agreement with similar results from Gianturco *et al* (1998) and Okamoto *et al* (1993) is very good. Experimental results (Johnstone and Newell 1991, Danjo and Nishimura 1985, Shyn and Cho 1987) are smaller over the whole energy range. As mentioned by Okamoto *et al* (1993), this is probably due to incorrect extrapolation of the differential cross sections to the forward direction needed since experiments were unable to properly measure the cross section both for small and large

Table 2. Symmetry, main configuration, parent state, resonance position, E_r, and resonance width, Γ_r, in eV: this paper, Belič *et al* (1981) (A), Morgan (1998) (B) and Gil *et al* (1994) (C).

			This paper		A	B		C	
Sym.	Main configuration	Parent state	E_r^a	Γ_r^a	E_r	E_r	Γ_r	E_r	Γ_r
$^2B_1$	$1b_1^{-1}4a_1^2$	$1\,^3B_1$	6.994	0.004	6.5	6.785	0.01	8.2	—
$^2A_1$	$3a_1^{-1}4a_1^2$	$1\,^3A_1$	9.151	0.010	8.6	8.81	0.02	10.5	≈0.2
$^2B_2$	$1b_2^{-1}4a_1^2$	$1\,^3B_2$	≈12.97	≈0.1	11.8	12.70	0.08	—	—

angles. The theoretical results of do N Varella *et al* (1999) agree better with experiment but they neglected target polarization.

We find a resonance of $^2B_1$ ($^2A''$ in C_s) symmetry below the first energy threshold that can be seen as a small peak in the elastic cross sections around 7 eV. Its position and width are shown in table 2 together with results from previous calculations and experiments. It is clear from our calculations that, in agreement with Belič *et al*, this is a Feshbach resonance whose main configuration and parent state are $1b_2^{-1}4a_1^2$ and $1\,^3B_1$ (see figure 4(*a*)), respectively. Morgan finds it at lower energies, in better agreement with experiment; Gil *et al* find it above the first excitation threshold, but they argue that adjusting this threshold would bring it down around 1 eV. Since our threshold is already smaller than the recommended value of Winter *et al* (1975), it is highly unlikely that adjusting it would bring the resonance position down.

The cross sections for excitation into the four lowest electronic states all have similar magnitude. The most noticeable difference between them is the presence of a sharp threshold for the (dipole-forbidden) transitions into the triplet states. The cross section for excitation into the state $1\,^3B_1$ is shown in figure 3. The results for models (*a*) and (*b*) are very similar and they agree better with those of Gil *et al* (1994) than with Morgan's which show a wide peak at about 10 eV. This is somewhat surprising since Gil *et al*'s calculation is simpler and fairly different from ours, whereas Morgan used the same methodology and a similar model to describe the target and target plus electron wavefunctions. The main difference between Morgan's calculation and ours is the basis set used to obtain the target molecular orbitals: Morgan used exactly the same one as Gil *et al*. We performed some tests using that basis set and concluded that the peak at 10 eV in Morgan's results is an artefact of calculation due to the amplitudes of some target wavefunctions being non-zero outside the *R*-matrix box. We therefore removed the most diffuse functions from the basis set and used a smaller one.

Our cross section shows a resonance at 9.15 eV for both models. This is a $^2A'$ Feshbach resonance ($^2A_1$ in C_{2v} symmetry) that is observed at 8.6 eV by Belič *et al* (1981) who attribute it the same main configuration, $3a_1^{-1}4a_1^2$. Morgan finds it at lower energies, in better agreement with the experimental value (see table 2) but identifies it as a core excited shape resonance. Gil *et al* see it at higher energies, and again they argue that adjusting for the error in their threshold energy by 1.2 eV brings it down to 9.3 eV. Once more our threshold is slightly lower than the recommended one. Our cross sections shows some structure in the 12–13 eV region. This is probably due to the presence of a $^2A'$ ($^2B_2$ in C_{2v}) resonance that is a clearly visible feature in the cross sections for excitation into the $^{3,1}A'$ states. The very small bump around 12.3 eV in the nine-state calculation is probably related to the $1\,^3A_2$ state, whose threshold energy is 12.338 eV.

In the case of the cross section for excitation into the $^1B_1(\tilde{A})$ state, there are some differences between the seven- and nine-state calculations: their shape is different in the 8–13 eV region. For higher energies both cross sections show similar behaviour but their magnitude differs by about 20%. The resonances (seen as small peaks) appear at the same

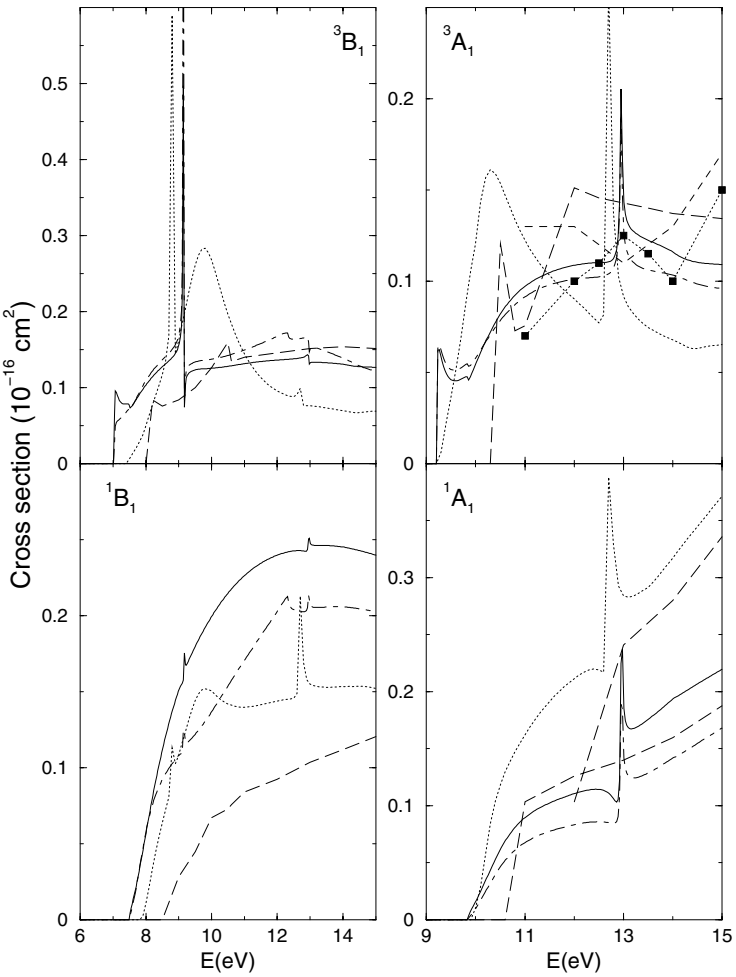

Figure 3. Fixed-nuclei cross sections for excitation into the four lowest excited states of H_2O indicated in the figures. Full curves: this paper, model (*a*); chain curve: this paper, model (*b*); dotted curve: Morgan (1998); long-dashed curve: Gil *et al* (1994); broken curve: Pritchard *et al* (1990) and dotted curve with squares: Lee *et al* (1993).

energies for both calculations: 12.97 eV for the abovementioned $^2B_2$ resonance and 9.15 eV for the $^2A_1$. Our cross sections are significantly bigger than those of Morgan and Gil *et al* in the whole energy range. Shifting the threshold to its recommended value of 7.49 eV slightly increased Morgan's cross section: it still remained smaller than ours.

For excitation into the 1 $^3A_1$ state, once again the seven- and nine-state calculations give similar results (see figure 3). This is the cross section for which the largest number of results is available. Although all of them have similar magnitude to ours, there is little agreement on its shape. Both Pritchard *et al* (using the Schwinger method) and Lee *et al* (distorted wave calculation) performed two-state calculations. The discrepancies between their results show that the differences between their and other cross sections is not only due to the number of states. The $^2A'$ ($^2B_2$) resonance at 12.97 eV is clearly visible in this cross section. Morgan finds this resonance at slightly lower energies, in better agreement with experimental results

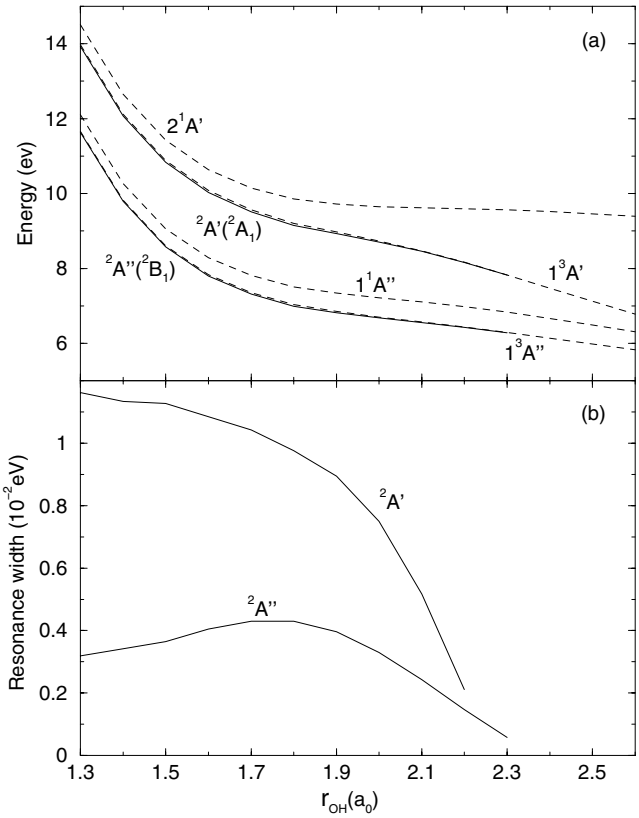

Figure 4. Resonance positions (*a*) and widths (*b*) as a function of the OH bond length for the resonances indicated in the figure. (*a*) Broken curves: threshold energies of the four lowest excited states; full curves: resonance positions as differences from the ground state equilibrium energy.

(see table 2). We believe this to be a Feshbach resonance, in accordance with Belič *et al* who, like us, attribute it the $1b_2^{-1}4a_1^2$ configuration.

Finally, the cross section for excitation to the $^1A_1(\tilde{B})$ state is shown in figure 3. Our cross sections for both models are again very similar in shape, with a maximum 20% difference in the magnitude at 15 eV. Morgan's cross section is significantly bigger than ours: almost twice as big at 15 eV. Gil *et al* have performed two calculations generating the IVO orbital in two different ways. The calculation they feel is more reliable is in better quantitative agreement with that of Morgan for high energies, whereas the other agrees better with our results for the whole energy range. Once again, the $^2A'$ resonance is clearly visible at 12.97 eV.

Summing up the differences between seven- and nine-state calculations, the $^1B_1(\tilde{A})$ is the only cross section that shows a difference in its shape. The differences in the magnitudes of the other cross sections are never larger than 20%. Therefore, since the use of the seven-state basis set with $a = 10$ is computationally cheaper, we have opted for it in the AN calculation.

In figure 4 we have plotted the position and width of the $^2B_1$ and $^2A_1$ resonances as a function of the OH bond length. Figure 4(*b*) shows that the width of the $^2A''$ ($^2B_1$) resonance has a maximum at the equilibrium OH bond length whereas the width of the $^2A'$ ($^2A_1$) resonance decreases with increasing OH distance. The position of the resonances follows very closely the energies of the $1\ ^3A''$ and $1\ ^3A'$ states. For r_{OH} larger than 2.3 the two resonances become

very narrow and we are unable to fit them. We were unable to fit the $^2B_2$ resonance for all bond lengths because it is too close to the $1\ ^3B_2$ threshold. Indeed, we believe that this resonance is probably not accurately described in our calculations since its parent state, the $1\ ^3B_2$, is not well represented. Regardless of this, we have manually fitted the eigenphase to a Breit–Wigner profile and found the approximate position and width for the equilibrium geometry.

4.2. Adiabatic nuclei results

To perform the AN calculation we assume that initially the H_2O is in its ground vibrational state. We use the T-matrices for 14 different geometries obtained using model (*a*) (seven states and $a = 10$) and changing r_{OH} from 1.3 to 2.6 in steps of 0.1. To test the convergence of the cross sections with the range of OH distances, we performed an initial 12-geometries calculation over the range [1.4; 2.5]: differences between both sets of cross sections were negligible.

The most significant feature of the AN cross sections is the fact that they are different from zero below the equilibrium fixed-nuclei thresholds. This result is, of course, impossible to obtain in a fixed-nuclei calculation. For the singlets, the cross section starts to be sizeable less than 0.5 eV below the fixed-nuclei (vertical) threshold. In the case of the triplets, it is around 1 eV below it. The larger effect on the triplets is due to the sharp onset of the cross sections for dipole-forbidden transitions. In principle, the dissociation cross section should be different from zero when the energy of the incoming electron is larger than the dissociation energy D_ν (in this case 5.2 eV for $\nu = 0$). But the threshold observed experimentally (called the effective Franck–Condon threshold) is different because it depends on the overlap between the initial and final vibrational wavefunctions. We find this effective threshold at $\approx$6 eV (see figure 6) which appears consistent with the results of Harb *et al* (2001).

The AN cross section for excitation into $1\ ^3A''$, plotted in figure 5, is similar to the fixed-nuclei one, but a bit smaller for all energies higher than the threshold energy. The adiabatic approximation does not treat resonances correctly so the resonance is averaged out when the nuclear motion is included in the calculations. The $^1A''(\tilde{A})$ AN cross section is also similar to the fixed-nuclei one: the shape is very similar, with the AN cross section being slightly smaller for $E > 9$ eV.

In contrast, the AN cross sections for the $1\ ^3A'$ and $^1A'(\tilde{B})$ states differ more significantly from the fixed-nuclei ones. In the case of $1\ ^3A'$, the AN cross section is much larger over the whole energy range (see figure 5) whereas the $^1A'(\tilde{B})$ one is smaller over the whole range. This last cross section also shows the smallest below vertical threshold values. The explanation for this can be found in the behaviour of the electronic energies of these states as a function of the internuclear separation and the effect this has on the nuclear continuum wavefunctions. For the $^1A'(\tilde{B})$ state, these functions have many more maxima and nodes in the [1.3; 2.6] range than the corresponding functions for the other states. This will have the effect of cancelling the fixed-nuclei cross sections, thus giving a smaller AN one. The case of the $1\ ^3A'$ is exactly the opposite, with fewer maxima and nodes, making the AN cross section bigger than the fixed-nuclei one.

4.3. Comparison with experiment. Limitations of our method

Figure 6 shows the total cross section for electron impact dissociative excitation measured by Harb *et al* (2001) who performed laser-induced fluorescence measurements of $OH(X\ ^2\Pi)$ production. According to them, the $1\ ^3A_1$ and $^1A_1(\tilde{B})$ states yield $OH(A\ ^2\Sigma)$. For this reason we have plotted in figure 6 the sum of the AN cross sections for excitation into the $1\ ^3B_1$ and $^1B_1(\tilde{A})$ states as well as the sum of the cross sections for the four lowest states of water. Our results and those of Morgan (1998) are much larger than the experimental results in the whole

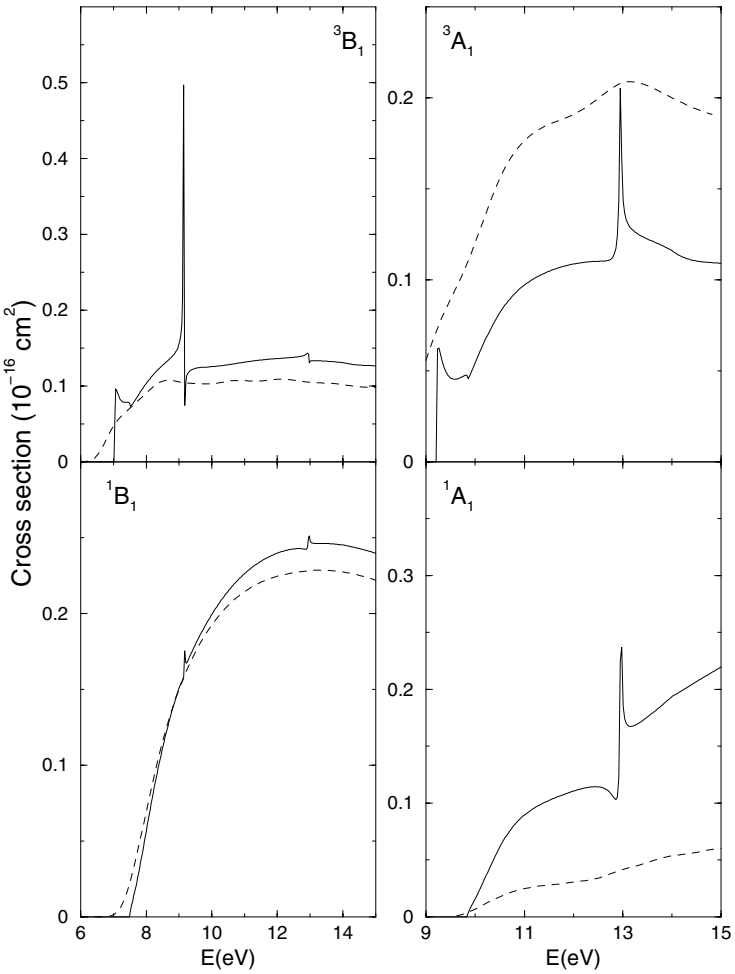

Figure 5. Total cross sections for excitation into the four lowest excited states of H_2O indicated in the figures. Full curves: fixed-nuclei calculation; broken curve: AN calculation. Both calculations performed using model (*a*).

energy range. The total cross section of Gil *et al* (1994) seems to be in better agreement with experiment but this is due to their thresholds being too high.

The discrepancy between theory and experiment may be due to the limitations of our calculation: the overestimation of the cross section may be attributable to the use of a one-dimensional model to treat the nuclear motion. A full three-dimensional treatment would allow other processes, including both relaxation and other dissociation paths, to take place, thus reducing the probability that flux goes into the OH + H channel. Avoided crossing, which cannot be treated in the AN approximation, could become relevant. For example, there is a well known conical intersection that plays an important role in photodissociation dynamics (see van Harrevelt and van Hemert (2000b)).

Furthermore, it is well known that the AN approximation fails in the proximity of resonances. The resonances found for water in the energy range treated in this paper are narrow and therefore long-lived. When this is the case, an accurate treatment of nuclear

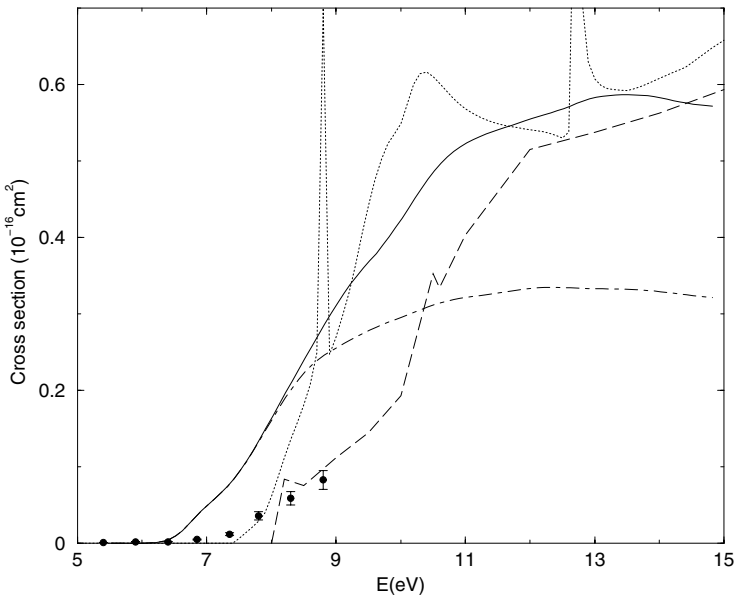

Figure 6. Comparison with experimental cross sections. Circles: direct dissociation measurements of Harb *et al* (2001). Full curve: sum of the four calculated excitation AN cross sections. Chain curve: sum of the $^3B_1$ and $^1B_1(\tilde{A})$ AN cross sections. Dotted curve: sum of Morgan's (1998) cross sections. Broken curve: sum of Gil *et al*'s (1994) cross sections.

motion in the resonant state potential energy surface is required. However, our model assumes that the dominant contribution to the dissociation cross section is non-resonant; the lack of structure in the experimental results could be taken as confirming this assumption. Finally, the use of the *R*-matrix method introduces a limitation in the diffuseness of the wavefunctions describing the target states. As a consequence the polarizability of the molecule may not be accurately reproduced and the quality of the representation of those states of Rydberg character is undermined.

5. Conclusions

We have calculated the electron impact dissociative excitation cross sections for the four lowest excited states of water using the energy balancing approximation. The cross sections calculated with this method have non-negligible values below the fixed-nuclei vertical threshold and, although the magnitudes of the cross sections for the 1 $^3A''$ and 1 $^1A''$ states are very similar to the fixed-nuclei ones, those of the 1 $^3A'$ and 2 $^1A'$ states differ significantly. The present calculations are the first to consider the nuclear motion in electron impact dissociation of a polyatomic molecule. Nevertheless, there is room for improvement: so far we have only attempted a one-dimensional calculation. It remains to be seen if a full three-dimensional study that would allow, for example, asymmetric distortion, will significantly alter the results.

Acknowledgments

This work was supported by the UK Engineering and Physical Sciences Research Council. We are grateful to J W McConkey for providing us with his results prior to publication.

References

Belič D S, Landau M and Hall R I 1981 *J. Phys. B: At. Mol. Phys.* **14** 175
Boudaiffa B, Cloutier P, Hunting D, Huels M A and Sanche L 2000 *Science* **287** 5458
Chase D M 1956 *Phys. Rev.* **104** 838
Chu S I and Dalgarno A 1974 *Phys. Rev.* A **10** 788
Curtis M G and Walker I C 1992 *J. Chem. Soc. Faraday Trans.* **88** 2805
Danjo A and Nishimura H 1985 *J. Phys. Soc. Japan* **54** 1224
do N Varella M T, Bettega M H F, Lima M A P and Ferreira L G 1999 *J. Chem. Phys.* **111** 6396
Dunning T H Jr 1970 *J. Chem. Phys.* **53** 2823
Dunning T H Jr 1971 *J. Chem. Phys.* **55** 716
Engel V, Staemmler V, Vander Wal R L, Crim F F, Sension R J, Hudson B, Andresen P, Hennig S, Weide K and Schinke R 1992 *J. Phys. Chem.* **96** 3201
Faure A, Gorfinkiel J D, Morgan L A and Tennyson J 2001 *Comput. Phys. Commun.* at press
Gianturco F A, Meloni S, Paioletti P, Lucchese R R and Sanna N 1998 *J. Chem. Phys.* **108** 4002
Gil T J, Rescigno T N, McCurdy C W and Lengsfield B H 1994 *Phys. Rev.* A **49** 2642
Hara S 1969 *J. Phys. Soc. Japan* **27** 1592
Harb T, Kedzierski W and McConkey J W 2001 *J. Chem. Phys.* **17** 123
Hwang D W, Yang X F, Harich S, Lin J J and Yang Y 1999 *J. Chem. Phys.* **110** 4123
Johnstone W M and Newell W R 1991 *J. Phys. B: At. Mol. Opt. Phys.* **24** 3633
Kimmel G A and Orlando T M 1995 *Phys. Rev. Lett.* **75** 2606
Kurawaki J, Ueki K, Higo M and Ogawa J 1983 *J. Chem. Phys.* **78** 3071
Lassetre E N, Skerbele A, Dillon M A and Ross K J 1968 *J. Chem. Phys.* **21** 145
Lee M T, Michelin S E, Machado L E and Brescansin L M 1993 *J. Phys. B: At. Mol. Opt. Phys.* **26** L203
Le Roy R J 1996 *University of Waterloo Chemical Physics Research Report* CP-555R
Melton C E 1972 *J. Chem. Phys.* **57** 4218
Mordaunt D H, Ashfold M N R and Dixon R N 1994 *J. Chem. Phys.* **100** 7360
Morgan L A 1998 *J. Phys. B: At. Mol. Opt. Phys.* **31** 5003
Morgan L A, Gillan C J, Tennyson J and Chen X 1997 *J. Phys. B: At. Mol. Opt. Phys.* **30** 4087
Morgan L A, Tennyson J and Gillan C J 1998 *Comput. Phys. Commun.* **114** 120
Nestmann B M and Peyerimhoff S D 1990 *J. Phys. B: At. Mol. Opt. Phys.* **23** L773
2001 NIST Standard Reference Database 69—July 2001 Release: NIST Chemistry WebBook, webbook.nist.gov/chemistry/
Okamoto Y, Onda K and Itikawa Y 1993 *J. Phys. B: At. Mol. Opt. Phys.* **26** 745
Pritchard H P, McKoy V and Lima M A P 1990 *Phys. Rev.* A **41** 546
Rountree P, Parentenau L and Sanche L 1991 *J. Chem. Phys.* **94** 8570
Schinke R 1993 *Photodissociation Dynamics* (Cambridge: Cambridge University Press)
Shugard M and Hazi A U 1975 *Phys. Rev.* A **12** 1895
Shyn T W and Cho S Y 1987 *Phys. Rev.* A **36** 5138
Stibbe D T and Tennyson J 1998a *New J. Phys.* **1** 2.1–2.9
Stibbe D T and Tennyson J 1998b *Comput. Phys. Commun.* **114** 236
Tennyson J 1996 *J. Phys. B: At. Mol. Opt. Phys.* **29** 6185
Tennyson J and Noble C J 1984 *Comput. Phys. Commun.* **32** 421
Trajmar S, Williams W and Kupperman A 1973 *J. Chem. Phys.* **58** 2521
Trevisan C S and Tennyson J 2001 *J. Phys. B: At. Mol. Opt. Phys.* **34** 2935
Tsurubichi S, Iwai T and Horie T 1974 *J. Phys. Soc. Japan* **36** 537
van Harrevelt R and van Hemert M C 2000a *J. Chem. Phys.* **112** 5777
van Harrevelt R and van Hemert M C 2000b *J. Chem. Phys.* **112** 5787
Winter N W, Goddard W A III and Bobrowicz F W 1975 *J. Chem. Phys.* **62** 4325
Yang X F, Hwang D W, Lin J J and Ying X 2000 *J. Chem. Phys.* **113** 10 597